

# Learning Task-Aware Effective Brain Connectivity for fMRI Analysis with Graph Neural Networks

Yue Yu<sup>†</sup>, Xuan Kan<sup>◊</sup>, Hejie Cui<sup>◊</sup>, Ran Xu<sup>◊</sup>, Yujia Zheng<sup>#</sup>, Xiangchen Song<sup>‡</sup>, Yanqiao Zhu<sup>§</sup>,  
Kun Zhang<sup>#,‡</sup>, Razieh Nabi<sup>\*</sup>, Ying Guo<sup>\*</sup>, Chao Zhang<sup>†</sup>, Carl Yang<sup>◊</sup>

<sup>†</sup>College of Computing, Georgia Institute of Technology

<sup>◊</sup>Department of Computer Science, <sup>\*</sup>Biostatistics and Bioinformatics, Emory University

<sup>#</sup>Department of Philosophy, <sup>‡</sup>Machine Learning, Carnegie Mellon University

<sup>§</sup>Department of Computer Science, University of California, Los Angeles

{yueyu, chaozhang}@gatech.edu,

{yujiazhang, xiangchensong, kunzhang}@cmu.edu,

yzhu@cs.ucla.edu,

{xuan.kan, hejie.cui, ran.xu, razieh.nabi, yguo2, j.carlyang}@emory.edu

**Abstract**—Functional magnetic resonance imaging (fMRI) has become one of the most common imaging modalities for brain function analysis. Recently, graph neural networks (GNN) have been adopted for fMRI analysis with superior performance. Unfortunately, traditional functional brain networks are mainly constructed based on similarities among region of interests (ROI), which are noisy and agnostic to the downstream prediction tasks and can lead to inferior results for GNN-based models. To better adapt GNNs for fMRI analysis, we propose TBDS, an end-to-end framework based on Task-aware Brain connectivity DAG (short for Directed Acyclic Graph) Structure generation for fMRI analysis. The key component of TBDS is the brain network generator which adopts a DAG learning approach to transform the raw time-series into task-aware brain connectivities. Besides, we design an additional contrastive regularization to inject task-specific knowledge during the brain network generation process. Comprehensive experiments on two fMRI datasets, namely Adolescent Brain Cognitive Development (ABCD) and Philadelphia Neuroimaging Cohort (PNC) datasets demonstrate the efficacy of TBDS. In addition, the generated brain networks also highlight the prediction-related brain regions and thus provide unique interpretations of the prediction results. Our implementation will be published upon acceptance<sup>1</sup>.

**Index Terms**—fMRI analysis, Brain Network, Direct Acyclic Graph Generation, Graph Neural Network

## I. INTRODUCTION

Human brains play a vital role in orchestrating complex neurological systems. Understanding the mechanisms of human brains has always been a core interest in the field of neuroscience and valuable to extensive downstream biomedical applications such as mental disorder therapy [58], neural system simulation [14], and cybernetic brain development [35]. Towards this goal, functional magnetic resonance imaging (fMRI) has been acknowledged as a valuable resource of information for brain investigation, which can reflect local changes in cerebral blood oxygenation evoked by sensory, motor, or cognitive tasks [8]. There has been a significant increase of interest in utilizing fMRI for brain connectome analysis, which

focuses on comprehending the brain organizations and their changes, identifying disease-specific biomarkers, as well as supporting clinical decisions such as biological sex prediction [42].

To leverage fMRI signals for neurological analysis, traditional biomedical research usually follows a two-stage approach [44]. In the first step, *functional brain networks* are generated from blood-oxygen-level-dependent (BOLD) time-series to model the interactions among regions of interests (ROIs). Then, the target classifier is stacked on top of the generated brain networks for downstream clinical predictions [18], [20], [24], [37]. Recently, end-to-end neural frameworks have been studied to generate *learnable brain networks* based on embedding similarity and make the prediction simultaneously [17], [56]. Thus the learned brain networks are more task-oriented under the supervision of task-specific objectives. However, two major shortcomings exhibit in both the traditional functional brain networks and the learnable ones. Firstly, these brain network generation methods focus on capturing the statistical associations between ROIs. Since correlation does not imply causation, they provide insufficient understandings of the complicated brain organization. Secondly, the connectivity in existing generated brain networks depends on the pairwise similarity between the time-series or embeddings of brain regions, which means that the constructed brain networks are fully or densely connected. The noisy signals contained in those dense networks hinder the identification of biological insights on the structure of brain networks and increase the time complexity of the downstream analysis.

Researchers have proposed a particular type of brain network, effective brain networks [7], which can overcome these two flaws. This type of brain network aims to infer causal relationships among brain regions and produce sparse connections [47]. To construct effective brain networks from BOLD signals, there are several mathematical algorithms available, including Granger causality [1], dynamic causal modeling [13], [16], autoencoders [19], and Bayesian search

<sup>1</sup>Will be uploaded to <https://github.com/yueyu1030/TBDS> in the future.

methods [39]. However, there are several major drawbacks in directly adopting these techniques for brain connectivity generation tasks: (1) *Unrealistic assumptions*: these methods often model the brain connectivity with overly simplistic assumptions, such as the absence of unmeasured confounding and lack of temporal dependencies. In reality, such assumptions are hard to satisfy. (2) *Limited scalability*: existing works based on constraint- or score-based methods for brain connectivity generation [9], [40] are usually evaluated on a selected ROI subset (less than 50 regions) for their difficulty on scalability. But in real application scenarios, there exist hundreds of ROIs, and directly adopting these methods could take several hours, or even several days for each instance. (3) *Difficulty of injecting task-specific information*: the above brain network generation methods are not customized for downstream clinical applications [19]. As a result, the mismatch between the network generation and downstream application would hurt the final performance and interpretation. Till now, generating effective and interpretable brain networks under the supervision of downstream tasks remains a challenging problem.

Fortunately, there is a recent trend in the machine learning community to view structure learning as a directed acyclic graphs (DAG) structure learning problem, which can be further converted to a continuous optimization constrained by additional structural regularizations to ensure acyclicity [30], [54], [57]. Then, this optimization can be solved with some gradient-based approaches, which are efficient, flexible, and can be integrated with other deep learning models.

Motivated by these studies, we propose TBDS, a task-aware brain network generation approach via modeling the connections among different ROIs as DAGs to identify effective brain connectivities and predict the target in an end-to-end fashion. To tackle the inscalability issue, we leverage the recently proposed approach [30], [57] and reformulate the DAG structure learning task as a gradient-based optimization problem, which could benefit from GPU acceleration and scales gracefully to hundreds of brain regions. In addition, to customize the generation process with downstream task knowledge, we design a contrastive loss [3], [55] to push the brain networks with the same label close and pull the brain networks with different labels apart [52]. Such a regularization enforces the brain networks from different classes to be more distinguishable, so that the downstream GNN classifier can learn to make better decisions. In this manner, we can optimize the brain networks towards the downstream tasks, and provide task-specific interpretations to support clinical predictions.

We evaluate TBDS on two real-world fMRI benchmarks datasets [2], [41] for the important and accessible task of biological sex prediction. The results illustrate that TBDS achieves competitive performance when compared with advanced baselines. Besides, TBDS is able to characterize the most important brain regions for the target tasks, justifying its efficacy on providing clinically useful interpretations.

## II. RELATED WORK

Two lines of the works are relevant to our study.

### A. fMRI-based Brain Network Analysis

Functional Magnetic Resonance Imaging (fMRI) encodes the blood oxygen level dependent (BOLD) signals, and has been widely used to discover the functional connectivity (FC) between different regions in the brain. To analyze the functional connectivity with fMRI, traditional methods include nonparametric permutation tests [21], [32], graph theory based methods [10], [38] and probabilistic graph modeling approaches [26]. However, these methods usually rely on hand-crafted features to infer the functional connectivity, and the generated brain networks are task-agnostic. With the rapid development of graph neural networks (GNNs), much attention has been paid to *GNN models for fMRI-based brain network analysis* [6], [24]. One major advantage of GNN-based models is that they are capable of aggregating node features based on graph structures and can be trained in an end-to-end fashion to solve downstream tasks.

However, GNNs usually require explicitly given graph structures and node attributes, which are often absent for fMRI analysis. To tackle this issue, some works directly use the brain networks constructed manually based on statistical correlations [45], but one drawback is that they cannot well handle the negative weights. Moreover, the statistical correlations are not specific to the downstream prediction tasks. Recently, there are some works that attempt to generate the brain networks and predict for the downstream tasks jointly [17], [23], [27]. But they are mainly based on structure similarity from GNNs [17] or attention weights [23], [27], which still cannot well characterize the complex relationships among different regions.

### B. DAG Structure Learning

Learning graphical structures based on Directed Acyclic Graphs (DAGs) is a fundamental problem in machine learning with a broad range of applications such as healthcare [25], [51], social networks [31] and biomedical informatics [43]. Traditional structure learning methods include constraint- and score-based methods, which test the validity of the generated graph with pre-defined scoring functions [4], [34] or constraints [28], [46]. However, one major drawback of such methods is the *computational inefficiency*, as the search problem is NP-hard [49] and the number of possible DAGs often increases super-exponentially with the number of nodes in the graph.

To reduce the computational overhead, [57] recasts the DAG search problem as a purely continuous optimization problem, where an additional penalty term is introduced to enforce the acyclicity of the generated graph. After that, many other works have extended this line of research [30], [33] to improve it both theoretically and empirically. Despite its effectiveness, DAG structure learning approaches are largely unexplored by current research for fMRI data. As recent works demonstrate the existence of causal links among different ROIs [12], [15],

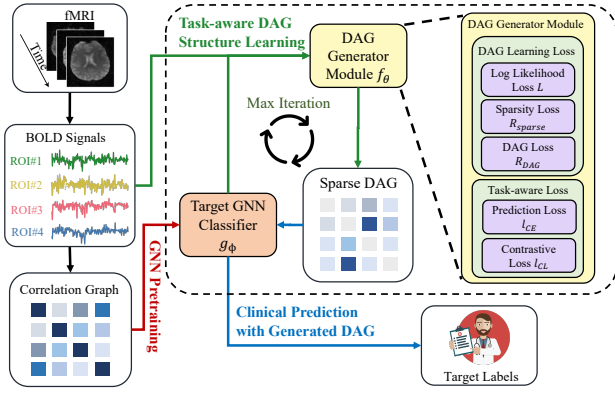


Fig. 1: The framework of TBDS. Different colors indicate different training stages.

[43], it is possible to leverage structure learning approaches to reveal the relations among different ROIs.

### III. METHOD

In this section, we first briefly summarize the task studied in this paper, then introduce the pipeline of using graph neural networks for prediction tasks on brain networks. Finally, we introduce how to leverage task-aware DAG learning techniques to generate effective brain connectivities.

#### A. Task Definition.

In this study, the input  $\mathbf{X} \in \mathbb{R}^{n \times v \times t}$  is the BOLD time-series for regions of interest (ROIs), where  $n$  is the sample size,  $v$  is the number of ROIs and  $t$  is the length of time-series. The target output for each time-series consists of two terms: (1) a functional brain network  $\mathbf{A} \in \mathbb{R}^{v \times v}$  (i.e., brain connectivity matrix) for each sample  $\mathbf{x} \in \mathbb{R}^{v \times t}$ , which serves as an intermediate result to the end-to-end framework. (2) the prediction  $\mathbf{Y} \in \mathbb{R}^{n \times |\mathcal{C}|}$ , where  $|\mathcal{C}|$  is the number of classes.

#### B. GNN for Brain Networks

Graph neural networks (GNNs) have been widely used in fMRI-based brain network analysis [5], [24], [53] due to their strong ability in learning node representations via propagating neighbor node features. However, one of the major challenges for adopting GNNs for brain networks is that they cannot handle edges with *negative weights* well. In this study, we leverage the *modified k-layer* graph convolutional network architecture [22] to accommodate negative edges in  $\mathbf{A}$  for clinical prediction tasks<sup>2</sup>. Let  $\Theta^{(k)} = (\theta_1^{(k)}, \theta_2^{(k)}, \dots, \theta_v^{(k)})$  be the matrix of all node embedding vectors at step  $k$ , the update rule for node embedding is

$$\Theta^{(k)} = \text{ReLU} \left( \hat{\mathbf{A}}_+ \Theta^{(k-1)} \mathbf{W}_+^{(k)} + \hat{\mathbf{A}}_- \Theta^{(k-1)} \mathbf{W}_-^{(k)} \right), \quad (1)$$

where  $\hat{\mathbf{A}}_+ = \mathbf{D}_+^{-\frac{1}{2}} (\mathbf{I} + \text{ReLU}(\mathbf{A})) \mathbf{D}_+^{-\frac{1}{2}}$  and  $\hat{\mathbf{A}}_- = \mathbf{D}_-^{-\frac{1}{2}} ((\mathbf{I} + \text{ReLU}(-\mathbf{A}))) \mathbf{D}_-^{-\frac{1}{2}}$  stands for the normalized adjacency matrices for positive edges and negative edges.  $\mathbf{D}_+ =$

<sup>2</sup>More complicated GNN structures can also be integrated with TBDS, which is of separate interests.

$\text{diag} \left( \sum_j \text{ReLU}(\mathbf{A})_{:,j} \right)$ ,  $\mathbf{D}_- = \text{diag} \left( \sum_j \text{ReLU}(-\mathbf{A})_{:,j} \right)$  is two diagonal matrices representing node degrees.  $\mathbf{W}^{(k)}$  stands for learnable parameters in convolutional layers and  $\Theta^{(0)} = \mathbf{F}$  is the *connection vector* that stands for Pearson correlation scores between its time-series with all the nodes contained in the brain network, which is suggested by [5]. After obtaining the node embeddings from the last GNN layer  $\Theta^{(k)}$ , we concatenate all the node embedding and use an additional classification head for the target prediction as

$$\hat{\mathbf{y}} = \sigma \left( \text{MLP} \left( \text{BatchNorm1D}(\|\theta_{j=1}^v \theta_j^{(k)}\|) \right) \right); \quad (2)$$

$$\mathcal{L}_{\text{tgt}} = \ell_{\text{CE}}(\hat{\mathbf{y}}, y), \quad (3)$$

where  $\hat{\mathbf{y}}$  is the probability simplex of the prediction and  $\sigma(\cdot)$  is the softmax function.

#### C. Task-aware DAG Structure Learning from BOLD Signals

◇ **Formulation.** For the input BOLD time-series  $\mathbf{x}$ , generating DAGs to capture the effective connectivities is not easy due to the complex spatio-temporal relationships among the ROIs: the current signal of a brain region is related to previous signals from both itself and other ROIs [29]. In this work, we hypothesize that different ROIs influence one another in both contemporaneous and time-lagged manner. Then, we harvest the standard SVAR model [48] to consider both spatial and temporal relationships during the DAG generation process. In the  $t$ -th step, the SVAR model can be expressed as

$$\mathbf{x}_t = \mathbf{A}^\top \mathbf{x}_t + \mathbf{A}_1^\top \mathbf{x}_{t-1} + \dots + \mathbf{A}_p^\top \mathbf{x}_{t-p} + \epsilon_t. \quad (4)$$

To interpret Eq. 4, we note that  $\mathbf{x}_t$  is an  $v$ -dimensional vector that represents the signal of all ROIs at the  $t$ -th step,  $\epsilon_t$  is a noise vector with independent elements [57], and  $p$  is the autoregressive order. Besides,  $\mathbf{A}_i$  ( $i = 1, 2, \dots, p$ ) represent weighted adjacency matrices with nonzero entries corresponding to the time-lagged relations, and  $\mathbf{A}$  is the directed acyclic graph (DAG) to model the effective relations among ROIs. To effectively model the BOLD signals among different time steps, we further assume the DAG structure is time-invariant and transform Eq. 4 into the matrix form as

$$\mathbf{X} = \mathbf{A}^\top \mathbf{X} + \mathbf{A}_1^\top \mathbf{X}_1 + \dots + \mathbf{A}_p^\top \mathbf{X}_p + \mathbf{E}, \quad (5)$$

where  $\mathbf{X}$  is a  $v \times (T + 1 - p)$  matrix with each column stands for one timestep and  $\mathbf{X}_1, \dots, \mathbf{X}_p$  are time-lagged versions of  $\mathbf{X}$ . Denote  $\mathbf{Z} = [\mathbf{X}_1 | \dots | \mathbf{X}_p]$  and  $\mathbf{B} = [\mathbf{A}_1^\top | \dots | \mathbf{A}_p^\top]^\top$ , we obtain the compact form of Eq. 5 as

$$\mathbf{X} = \mathbf{A}^\top \mathbf{X} + \mathbf{B}^\top \mathbf{Z} + \mathbf{E}. \quad (6)$$

◇ **Optimization Objective for Vanilla DAG Learning.** To learn the DAG structure for brain networks with  $\mathbf{X}, \mathbf{Z}$ , we aim to estimate the matrix  $\mathbf{A}$  and  $\mathbf{B}$  to satisfy Eq. 5 as well as the directed acyclic constraint (for  $\mathbf{A}$  only). This indeed creates a constraint optimization problem, written as follows

$$\min_{\mathbf{A}, \mathbf{B}} \ell(\mathbf{A}, \mathbf{B}) = \frac{1}{2} \|\mathbf{X} - \mathbf{A}^\top \mathbf{X} - \mathbf{B}^\top \mathbf{Z}\|_F^2 \quad \text{s.t. } \mathbf{A} \text{ is acyclic.} \quad (7)$$

Here  $\ell(\mathbf{A}, \mathbf{B})$  is the objective for DAG generation.

Directly optimizing Eq. 7 is difficult due to the hard acyclicity constraint [57]. To circumvent this issue, we follow the recent work [30] and reformulate the above task to an *unconstrained optimization problem* via applying additional *soft sparsity* and *acyclic* regularization for learning a DAG equivalent to the ground truth DAG. The overall objective function is defined as

$$\min_{\mathbf{A}, \mathbf{B}} S(\mathbf{A}, \mathbf{B}; \mathbf{X}) = \mathcal{L}(\mathbf{A}, \mathbf{B}; \mathbf{X}) \quad (8)$$

$$+ \lambda_1 (\mathcal{R}_{\text{sparse}}(\mathbf{A}) + \mathcal{R}_{\text{sparse}}(\mathbf{B})) \quad (9)$$

$$+ \lambda_2 \mathcal{R}_{\text{DAG}}(\mathbf{A}) \quad (10)$$

where

$$\mathcal{L}(\mathbf{A}, \mathbf{B}; \mathbf{X}) = -\frac{1}{2} \sum_{i=1}^v \log \left( \sum_{j=1}^{T+1-p} (\mathbf{X}_{i,j} - \mathbf{A}_i^\top \mathbf{X}_{:,j} - \mathbf{B}_i^\top \mathbf{Z}_{:,j})^2 \right) \quad (11)$$

$$+ \log |\det(\mathbf{I} - \mathbf{A})| + \text{const.} \quad (12)$$

$\mathcal{L}(\mathbf{A}, \mathbf{B}; \mathbf{X})$  is the learning objective of the maximum log-likelihood estimator of  $\mathbf{X}, \mathbf{Z}$  following multivariate Gaussian distribution. In addition, we use  $l_1$  penalty to approximate the sparse constraint and use the DAG constraint proposed in [57] as the realization of  $\mathcal{R}_{\text{DAG}}$  which can be written as

$$\mathcal{R}_{\text{sparse}}(\mathbf{A}) = \|\mathbf{A}\|_1, \quad \mathcal{R}_{\text{DAG}}(\mathbf{A}) = \text{tr}(e^{\mathbf{A} \circ \mathbf{A}}) - v. \quad (13)$$

By optimizing  $\mathbf{A}$  and  $\mathbf{B}$  with the above equations, we are able to obtain the brain network  $\mathbf{A}$ , which will be also used in the downstream task described as follows.

◇ **Task-aware DAG Structure Learning.** The previous sections have not fully explore the connections between the DAG generation model as  $\mathbf{A} = f_\theta(\mathbf{X})$ , and the target prediction model as  $\hat{\mathbf{y}} = g_\phi(\mathbf{A}, \mathbf{F})$ . In this work, we aim to establish the connection between  $f_\theta(\mathbf{X})$  and  $g_\phi(\mathbf{A}, \mathbf{F})$  by leveraging  $g_\phi(\mathbf{A}, \mathbf{F})$  to guide the structure learning process.

To achieve this, we first pretrain the  $g_\phi$  on the training set by setting  $\mathbf{A} = \mathbf{F}$ . In this way, the brain connectivity is initialized with the Pearson correlation matrix, which reflects statistical correlations among nodes. Such connectivities could serve as a warmup for the training of  $g_\phi$ . We denote the pretrained model as  $g_\phi^{(0)}$ . With an estimated target classifier from  $g_\phi$ , TBDS trains the generator  $f_\theta(\mathbf{X})$  to generate *more discriminative* DAGs easier for  $g_\phi(\mathbf{A}, \mathbf{F})$  to classify. The learning objective of the task-aware DAG structure learning can be written as

$$\min_{\mathbf{A}, \mathbf{B}} \mathcal{L}_{\text{Gen}} = S(\mathbf{A}, \mathbf{B}; \mathbf{X}) + \mu (\ell_{\text{CE}}(g_\phi(\mathbf{A}, \mathbf{F}), y) + \ell_{\text{CL}}(g_\phi(\mathbf{A}, \mathbf{F}), y)), \quad (14)$$

where  $\mu$  is a hyperparameter to control the weight of two regularization terms, and  $\ell_{\text{CL}}$  is the contrastive loss. Note that in this step, we keep  $g_\phi$  fixed without updating its parameters. To calculate  $\ell_{\text{CL}}$ , we first calculate the representation for each

---

**Algorithm 1** The training procedure of TBDS.

---

**Input:** BOLD time series  $\mathbf{X}$ , Pearson Correlation Matrix  $\mathbf{F}$   
**Output:** Brain Network  $\mathbf{A}$ , prediction  $\hat{\mathbf{y}}$ , DAG generation module  $f_\theta$ , target GNN classification module  $g_\phi^0$ .

1:  $i = 0$ .

2: // *Training Stage*

3: Pretrain  $g_\phi$  via setting  $\mathbf{A} = \mathbf{F}$  (Eq. 1- 3).

4: **while**  $i < \text{MaxIter}$  **do**

5:   Generate  $\mathbf{A}^{(i)}, \mathbf{B}^{(i)}$  on the training set using  $g_\phi^{(i-1)}$  (Eq. 14).

6:   Train  $g_\phi^{(i)}$  with the generated  $\mathbf{A}^{(i)}$  (Eq. 1- 3).

7:    $i = i + 1$ .

8: **end while**

9: // *Inference Stage*

10: Generate  $\mathbf{A}, \mathbf{B}$  on the test set with pseudo labels derived from  $g_\phi^{(i)}$  (Eq. 16).

11: Inference the labels  $\hat{\mathbf{y}}$  on the test set with  $g_\phi^{(i)}$  (Eq. 1- 2).

---

DAG as  $\mathbf{v} = \text{GNN}(\mathbf{A}) \in \mathbb{R}^d$  (the architecture of GNN is in Eq. 1.). Then, we use the margin-based contrastive loss as

$$\ell_{\text{pos},i} = \frac{\sum_{p \in \mathcal{P}_i} \|\mathbf{v}_i - \mathbf{v}_p\|^2}{|\mathcal{P}_i|}, \quad \ell_{\text{neg},i} = \frac{\sum_{n \in \mathcal{N}_i} (\xi - \|\mathbf{v}_i - \mathbf{v}_n\|)^2}{|\mathcal{N}_i|},$$

$$\ell_{\text{CL}} = \sum_{i=1}^M \frac{1}{dM} (\ell_{\text{pos},i} + \ell_{\text{neg},i}). \quad (15)$$

Here  $M$  is the number of DAGs in a batch,  $\mathcal{P}_i$  and  $\mathcal{N}_i$  is the set of instances from the same or different class from  $i$ -th instance, respectively.

We remark that  $\ell_{\text{CE}}$  and  $\ell_{\text{CL}}$  optimize the DAG generation from different perspectives:  $\ell_{\text{CE}}$  directly optimizes over the final prediction, while  $\ell_{\text{CL}}$  operates on the representation space to push the embeddings of DAGs from the same class close and pull the embeddings from different classes further apart [55]. By injecting these two terms, we are able to generate task-specific DAGs to better support the clinical prediction tasks.

◇ **Inference on Test Data.** One challenge for the method mentioned above is that for *test data*, we do not have any ground truth label  $y$ , thus directly using Eq. 14 is infeasible. To tackle this issue, we propose to leverage the *pseudo labels* predicted from  $\tilde{\mathbf{y}} = \arg \max(\hat{\mathbf{y}})$  as a substitute of the ground truth labels. Then, to suppress the label noise in pseudo labels, we add an additional reweighting term via leveraging the predictive uncertainty  $\omega_{\mathbf{A}} = 1 - \text{Entropy}(\hat{\mathbf{y}}) = 1 - \sum_i \hat{\mathbf{y}}_i \log \hat{\mathbf{y}}_i$ .

In this way, if the model is *certain* about its prediction, the entropy would be low, and we assign higher weight for two additional terms to encourage the model to learn from the target tasks. In contrast, when the model prediction is uncertain indicating that it is more possible to be erroneous, we reduce the weight to prevent it from overfitting to the noise. The

overall learning objective for test data is expressed below.

$$\min_{\mathbf{A}, \mathbf{B}} \mathcal{L}_{\text{Gen, test}} = \mathcal{S}(\mathbf{A}, \mathbf{B}; \mathbf{X}) + \mu \cdot \omega_{\mathbf{A}} (\ell_{\text{CE}}(g_{\phi}(\mathbf{A}, \mathbf{F}), \hat{y}) + \ell_{\text{CL}}(g_{\phi}(\mathbf{A}, \mathbf{F}), \hat{y})), \quad (16)$$

#### D. End-to-end Training

The overall procedure of TBDS is shown in Alg. 1. It is worth noting that the two modules  $f_{\theta}$  and  $g_{\phi}$  are trained in an end-to-end way, as the label  $y$  and the task-oriented graphs are leveraged simultaneously. Moreover, the brain networks of the test set are inferred *separately* from the training set. Thus, we eliminate the issue of information leakage, as *no information* from the test set has been used during the tuning process.

### IV. EXPERIMENTS

In this section, we conduct extensive experiments to answer the following three research questions: **RQ1**: How does TBDS perform as compared with state-of-the-art methods? **RQ2**: How do the key designs in TBDS affect performance? **RQ3**: Does the generated brain connectivity by TBDS offers reasonable interpretability for target prediction tasks?

#### A. Experiment Setup

◇ **Dataset.** We conduct experiments demonstrating the utility of TBDS using two real-world fMRI datasets.

(a) *Philadelphia Neuroimaging Cohort (PNC)* is a dataset curated from a collaborative project from the Brain Behavior Laboratory at the University of Pennsylvania and the Children’s Hospital of Philadelphia. It includes a population-based sample of individuals aged 8–21 years [41]. After quality control, we utilize rs-fMRI data of 503 subjects, with 289 (57.46%) of them being females. The nodes are grouped into 10 functional modules that correspond to major resting-state networks. In the resulting data, each sample contains 264 nodes with time-series data collected through 120 time steps.

(b) *Adolescent Brain Cognitive Development Study (ABCD)* [2] is one of the largest publicly available fMRI datasets. This study is recruiting children aged 9–10 years across 21 sites in the U.S. Each child is followed into early adulthood, with repeated imaging scans as well as extensive psychological and cognitive testing. After quality control, the dataset include fMRI data of 7901 children, and 3961 (50.1%) among them are female. After processing, each sample contains 360 nodes. Only samples with at least 512 time points are selected, and the first 512 time points are included in the dataset.

◇ **Task.** We choose biological sex prediction as the evaluation task since sexuality is an essential aspect of adolescent development, biological sex prediction is a critical and meaningful task for ABCD and PNC. Many papers [17], [36], [42] have focused on this task using brain networks.

◇ **Evaluation Metrics.** As the label distributions of both PNC and ABCD datasets are balanced, we use both *AUROC* and *accuracy* as the performance metrics. For accuracy, we use 0.5 as the threshold after obtaining the predicted result.

◇ **Implementations.** We implement our model in PyTorch<sup>3</sup>. We use Adam as the optimizer with the learning rate 1e-4. The key hyperparameters in TBDS include regularization weight  $\lambda_1, \lambda_2, \mu$  and the number of steps  $p$  in SVAR model. Following common practice [30], we set  $\lambda_1 = 1, \lambda_2 = 10, \mu = 10$  without further tuning. Following [40], we set  $p = 3$  as further increasing  $p$  will introduce more learnable parameters which causes OOM error for large datasets (ABCD). MaxIter is set to 3 for PNC and 2 for ABCD as we find increasing the number iteration will not significantly increase the model’s performance but extend the running time.

#### B. Baselines

We compare TBDS with the following baselines:<sup>4</sup>

(a) **Time-series based Models.** These baselines model BOLD time-series data *without* networks. Here we select *bi-GRU* as the baseline to encode BOLD time-series.

(b) **Statistical Methods for Brain Networks.** These baselines use statistical methods to construct brain networks, including *uniform graphs*, which sets all entries in adjacency matrices with one and *Pearson correlation graphs*, which sets the weight in adjacency matrices as Pearson correlation of BOLD signals. To enable fair comparison, we use the same node features and GNN predictor as TBDS for prediction.

(c) **Deep Learning Models for Brain Networks.** We also compare our method with four popular deep models for brain networks, *BrainnetCNN* [20], *BrainGNN* [24], *SAN* [23], and *BrainGB* [5]. Note that these methods develops advanced neural networks with the fixed correlation-based functional brain networks to model the relations among different ROIs.

(d) **Models with Learnable Brain Network Generation.** We introduce three other baselines based on learnable graph generators, namely *LDS* [11], *FBNetGen* [17] and *GNN-DAG* [40]. LDS is a framework which jointly learns graph structures and model parameters through bilevel optimization. FBNetGen is an end-to-end approach for learning task-aware brain networks based on embedding similarities. GNN-DAG leverages causal discovery algorithm [39] for generating brain networks. Note that the original GNN-DAG method is not designed for downstream tasks, and we use the same GNN classifier to adapt GNN-DAG for target tasks.

#### C. Main Experiment (RQ1)

From the experimental results shown in Table I, we have the following findings:

- TBDS outperforms all the baselines for the PNC dataset with 3% performance gain. On the ABCD dataset, it achieves competitive performance when compared with the strongest baseline (FBNetGen). This is because ABCD is a much larger dataset (16 times larger than PNC) with plenty of labels, and directly using embedding similarity is sufficient for capturing the relations among ROIs. Conversely, when labeled data is limited, FBNetGen cannot perform as

<sup>3</sup><https://pytorch.org/>

<sup>4</sup>To ensure fair comparison, we tune the parameter for TBDS and baselines and choose the best one based on the performance of the development set.

| Type              | Method           | Dataset: PNC      |                   | Dataset: ABCD     |                   |
|-------------------|------------------|-------------------|-------------------|-------------------|-------------------|
|                   |                  | AUROC             | Accuracy          | AUROC             | Accuracy          |
| Time-series       | bi-GRU           | 65.1 ± 3.5        | 58.1 ± 2.4        | 51.2 ± 1.0        | 49.9 ± 0.8        |
| Traditional Graph | GNN-Uniform      | 70.6 ± 4.8        | 66.2 ± 3.9        | 88.8 ± 0.7        | 80.5 ± 0.7        |
|                   | GNN-Pearson      | 76.5 ± 2.7        | 69.2 ± 1.8        | 91.0 ± 0.5        | 82.4 ± 0.5        |
| Deep Model        | BrainnetCNN [20] | 78.5 ± 3.2        | 71.9 ± 4.9        | 93.5 ± 0.3        | 85.7 ± 0.8        |
|                   | BrainGNN [24]    | 77.5 ± 3.2        | 70.6 ± 4.8        | OOM               | OOM               |
|                   | SAN [23]         | 73.0 ± 1.6        | 70.4 ± 2.4        | 90.1 ± 1.2        | 81.0 ± 1.3        |
|                   | BrainGB [5]      | 76.6 ± 5.0        | 69.8 ± 4.2        | 91.8 ± 0.3        | 83.1 ± 0.9        |
| Learnable Graph   | LDS [11]         | 78.2 ± 3.8        | 70.8 ± 6.2        | 90.7 ± 0.3        | 82.5 ± 0.9        |
|                   | FBNetGen [17]    | 80.8 ± 3.3        | 74.8 ± 2.3        | <b>94.5 ± 0.7</b> | 87.2 ± 1.2        |
|                   | GNN-DAG [40]     | 80.5 ± 2.6        | 72.3 ± 2.0        | > 1 week          | > 1 week          |
| Ours              | TBDS             | <b>83.4 ± 1.9</b> | <b>76.9 ± 1.8</b> | 94.2 ± 0.2        | <b>88.0 ± 0.4</b> |

TABLE I: Performance (in %) comparison with different types of baselines. Note that **OOM** means out-of-memory error, and **>1 week** means the algorithm cannot be finished in 1 week. PNC is a *low-resource* dataset including 503 fMRI data, ABCD is a *high-resource* dataset including 7901 fMRI data.

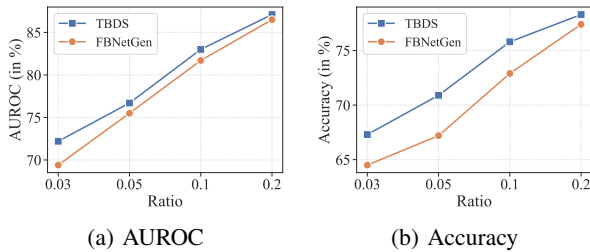


Fig. 2: Performance of TBDS and FBNetGen trained with different fractions of labeled data in ABCD training set.

well as TBDS. To further validate this point, we run TBDS and FBNetGen on a subset of ABCD with different fraction of labeled data ( $\{3\%, 5\%, 10\%, 20\%\}$ ). As shown in Fig. 2, TBDS continuously outperform FBNetGen, which justifies the efficacy of TBDS under low-data regime.

- Directly using statistical correlations as brain connectivity is insufficient to capture the relationships among ROIs, as they achieve suboptimal results on two datasets. Designing more complicated GNN architectures does not address this challenge — baselines with carefully designed GNN models [5], [20], [23] still underperform TBDS on two benchmarks.
- Previous methods leveraging DAG generation approaches can outperform statistical-based brain network generation methods. However, the biggest obstacle is the time complexity — generating brain networks on larger datasets often takes too much time. Such an inefficiency issue hinders it from being deployed in real applications. In TBDS, we use continuous optimization techniques with GPU acceleration, which reduce the overall running time significantly (1.5 hours for PNC and 5 hours for ABCD).

#### D. Performance Analysis (RQ2)

◇ **Ablation Studies.** We further examine the designed components in our graph generation (Section III-C): the cross-entropy loss from the target task  $\ell_{CE}$  (Eq. 14), the contrastive

| Dataset | TBDS              | w/o $\ell_{CE}$ | w/o $\ell_{CL}$ | w/o $\omega_A$ | w/o E2E    | w/o NE     |
|---------|-------------------|-----------------|-----------------|----------------|------------|------------|
| PNC     | <b>83.4 ± 2.0</b> | 82.6 ± 1.4      | 81.8 ± 1.5      | 82.6 ± 1.8     | 81.0 ± 1.8 | 71.2 ± 2.9 |
| ABCD    | <b>94.2 ± 0.2</b> | 93.7 ± 0.5      | 93.8 ± 0.4      | 93.5 ± 0.3     | 92.8 ± 0.6 | 88.5 ± 2.6 |

TABLE II: Ablation study: AUROC performance on two datasets after removing specific components.

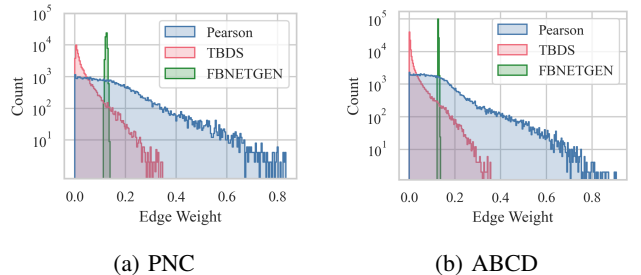


Fig. 3: Weight density distributions of the generated brain networks. TBDS produces much sparser brain connectivities.

loss  $\ell_{CL}$  (Eq. 14), the uncertainty-aware weight for test data  $\omega_A$  (Eq. 16), the whole end-to-end learning process (E2E)<sup>5</sup>, and the strategy for handling negative weight (Eq. 1). From Table II, we find that all these components contribute to the final performance. Removing  $\ell_{CE}$  and  $\ell_{CL}$  results in performance degradation, as they focus on different parts of the task knowledge (predictions and representations respectively). The *uncertainty-based reweighting*  $\omega_A$  prevents the generative model from overfitting to the noise of the target classifier, and leads to overall better performance. Combining them in TBDS provides the best overall effectiveness. *End-to-end learning* makes our learning framework more flexible, thus leads to 2.2% performance gain on average. Our proposed strategy for *tackling negative edges* in Eq. 1 effectively resolves the issue, which brings significantly performance gain (up to 17%).

<sup>5</sup>When removing E2E, the model first generates DAG via Eq. 8 to Eq. 10 then directly use the DAG for target task prediction via  $g_\phi$  (Eq. 1-2).



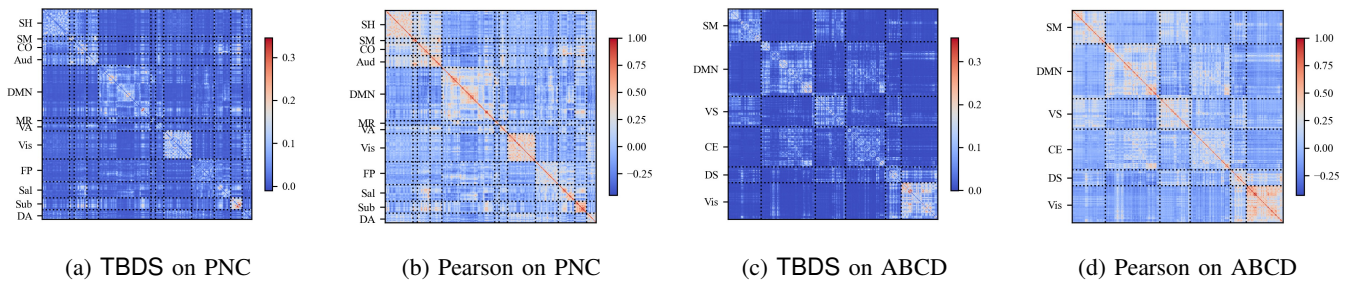


Fig. 4: Visualizations of brain connectivities generated via TBDS vs. Pearson. Warmer colors indicate higher values. The neural systems on PNC include Somatomotor Hand (SH), Somatomotor Mouth (SM), Subcortical (Sub), Visual (Vis), Auditory (Aud), Cingulo-opercular (CO), Salience (Sal), Default mode (DMN), Fronto-parietal (FP), Ventral attention (VA), Dorsal attention (DA), and Memory retrieval (MR). For ABCD, the neural systems include SM, DMN, Ventral salience (VS), Central executive (CE), Dorsal salience (DS), and Vis.

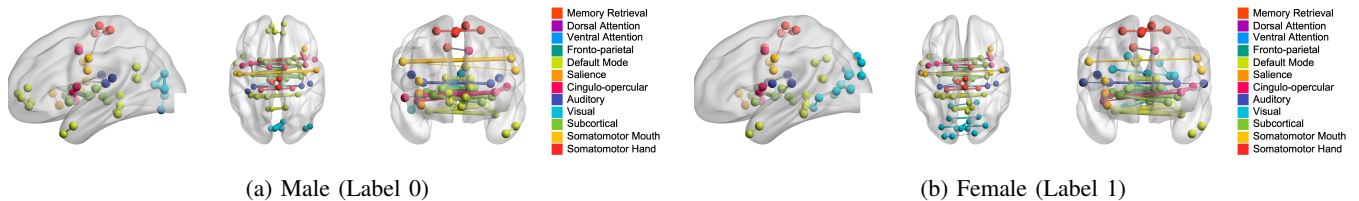


Fig. 5: Visualizations of predominant connectivities generated via TBDS on different biological sexes. Edges spanning multiple neural systems are colored gray, whereas those linking nodes within the same neural system are colored appropriately. Edge widths reflect the connectivity strengths.

◇ **Sparsity of the Generated DAGs.** Fig. 3 illustrates the connection weight distribution among different ROIs. It is shown that TBDS fulfills the purpose of sparsity, as most of the weights are close to zero. In contrast, the original Pearson correlation matrix contains many noisy edges and the brain connectivity is dense. FBNNetGen leverages dot product with softmax normalization to calculate the edge weights, but the softmax operation makes the variance of the edge weights smaller, and the generated graph is not sparse enough.

### E. Case Studies (RQ3)

We explicitly visualize the generated brain connectivities of TBDS and Pearson in Fig. 4. It clearly shows that our proposed task-aware DAG learning method generates much sparser connectivities compared with the correlation based method, which effectively controls the time complexity for downstream analysis. At the same time, the edge strength patterns observed in Pearson graphs remain in DAG sparse graphs, indicating that our method can highlight meaningful signals while suppressing random noise that may hinder the identification of potential biomarkers.

Furthermore, to demonstrate the class discrimination ability of our task-aware DAG brain connectivity, we visualize and compare the strong connections of the learned brain networks between two biological sex groups, as shown in Fig. 5. Specifically, we first divide the learned graphs based on their class labels and calculate an average network by taking the average weight of each edge within the same class. The top 100 most predominant edges are then visualized using

the BrainNet Viewer [50]. By comparing Fig. 5(a) and Fig. 5(b), we can observe that the main difference in important connections between different biological sex groups lies in the Default Mode Network (DMN), the Auditory Network (Aud) and the Visual Network (Vis), which is in line with previous studies [42] that ROIs with significant biological sex differences are located in the DMN and Aud systems. This indicates that our learnable brain connectivity is task-oriented and retains favorable class discrimination ability.

### V. CONCLUSION

In this paper, we propose TBDS, a task-aware effective brain connectivity generation approach to support clinical predictive tasks. In particular, we leverage the DAG structure learning techniques to encode the relations among ROIs, and add two additional regularizations to inject task-specific information. Our end-to-end framework is efficient with GPU acceleration. The experiments on two real-world datasets illustrate the superior performance of TBDS when compared with advanced baselines, and demonstrates valuable neurological interpretations towards downstream tasks.

### REFERENCES

- [1] L. Barnett and A. K. Seth, “The mvgc multivariate granger causality toolbox: a new approach to granger-causal inference,” *Journal of neuroscience methods*, 2014.
- [2] B. Casey, T. Cannonier, and M. I. C. et al., “The adolescent brain cognitive development (abcd) study: Imaging acquisition across 21 sites,” *Developmental Cognitive Neuroscience*, 2018.
- [3] T. Chen, S. Kornblith, M. Norouzi, and G. Hinton, “A simple framework for contrastive learning of visual representations,” in *ICML*, 2020.

- [4] D. M. Chickering, "Optimal structure identification with greedy search," *Journal of machine learning research*, 2002.
- [5] H. Cui, W. Dai, Y. Zhu, X. Kan, A. A. Chen Gu, J. Lukemire, L. Zhan, L. He, Y. Guo, and C. Yang, "BrainGB: A Benchmark for Brain Network Analysis with Graph Neural Networks," *IEEE Trans Med Imaging*, 2022.
- [6] H. Cui, W. Dai, Y. Zhu, X. Li, L. He, and C. Yang, "Interpretable graph neural networks for connectome-based brain disorder analysis," in *MICCAI*, 2022.
- [7] G. Deshpande and X. Hu, "Investigating effective brain connectivity from fmri data: past findings and current issues with reference to granger causality analysis," *Brain connectivity*, 2012.
- [8] E. A. DeYoe, P. Bandettini, J. Neitz, D. Miller, and P. Winans, "Functional magnetic resonance imaging (fmri) of the human brain," *Journal of neuroscience methods*, 1994.
- [9] J. Dubois, H. Oya, J. M. Tyszka, M. Howard III, F. Eberhardt, and R. Adolphs, "Causal mapping of emotion networks in the human brain: Framework and initial findings," *Neuropsychologia*, 2020.
- [10] A. Fornito, A. Zalesky, and M. Breakspear, "Graph analysis of the human connectome: promise, progress, and pitfalls," *Neuroimage*, 2013.
- [11] L. Franceschi, M. Niepert, M. Pontil, and X. He, "Learning discrete structures for graph neural networks," in *ICML*, 2019.
- [12] K. Friston, "Causal modelling and brain connectivity in functional magnetic resonance imaging," *PLoS biology*, 2009.
- [13] K. J. Friston, L. Harrison, and W. Penny, "Dynamic causal modelling," *Neuroimage*, 2003.
- [14] F. Giralt, A. Arenas, J. Ferre-Gine, R. Rallo, and G. Kopp, "The simulation and interpretation of free turbulence with a cognitive neural system," *Physics of Fluids*, 2000.
- [15] C. A. Hill, S. Suzuki, R. Polania, M. Moisa, J. P. O'doherty, and C. C. Ruff, "A causal account of the brain network computations underlying strategic social behavior," *Nature neuroscience*, 2017.
- [16] C. J. Honey, R. Kötter, M. Breakspear, and O. Sporns, "Network structure of cerebral cortex shapes functional connectivity on multiple time scales," *PNAS*, 2007.
- [17] X. Kan, H. Cui, J. Lukemire, Y. Guo, and C. Yang, "FBNETGEN: Task-aware GNN-based fMRI analysis via functional brain network generation," in *MIDL*, 2022.
- [18] X. Kan, W. Dai, H. Cui, Z. Zhang, Y. Guo, and Y. Carl, "Brain network transformer," in *NeurIPS*, 2022.
- [19] A. Kascenas, N. Pugeault, and A. Q. O'Neil, "Denoising autoencoders for unsupervised anomaly detection in brain MRI," in *MIDL*, 2022.
- [20] J. Kawahara, C. J. Brown, S. P. Miller, B. G. Booth, V. Chau, R. E. Grunau, J. G. Zwicker, and G. Hamarneh, "BrainNetCNN: Convolutional neural networks for brain networks; towards predicting neurodevelopment," *NeuroImage*, 2017.
- [21] J. Kim, J. R. Wozniak, B. A. Mueller, and W. Pan, "Testing group differences in brain functional connectivity: using correlations or partial correlations?" *Brain connectivity*, 2015.
- [22] T. N. Kipf and M. Welling, "Semi-supervised classification with graph convolutional networks," in *ICLR*, 2017.
- [23] D. Kreuzer, D. Beaini, W. L. Hamilton, V. Létourneau, and P. Tossou, "Rethinking graph transformers with spectral attention," in *NeurIPS*, 2021.
- [24] X. Li, Y. Zhou, S. Gao, N. Dvornik, M. Zhang, J. Zhuang, S. Gu, D. Scheinost, L. Staib, P. Ventola *et al.*, "Braingnn: Interpretable brain graph neural network for fmri analysis," *Medical Image Analysis*, 2021.
- [25] P. J. Lucas, L. C. Van der Gaag, and A. Abu-Hanna, "Bayesian networks in biomedicine and health-care," *Artificial intelligence in medicine*, 2004.
- [26] J. Lukemire, S. Kundu, G. Pagnoni, and Y. Guo, "Bayesian joint modeling of multiple brain functional networks," *JASA*, 2021.
- [27] U. Mahmood, Z. Fu, V. D. Calhoun, and S. Plis, "A deep learning model for data-driven discovery of functional connectivity," *Algorithms*, 2021.
- [28] D. Maxwell Chickering and D. Heckerman, "Efficient approximations for the marginal likelihood of bayesian networks with hidden variables," *Machine learning*, 1997.
- [29] A. Mitra, A. Z. Snyder, C. D. Hacker, and M. E. Raichle, "Lag structure in resting-state fmri," *Journal of neurophysiology*, 2014.
- [30] I. Ng, A. Ghassami, and K. Zhang, "On the role of sparsity and dag constraints for learning linear dags," *NeurIPS*, 2020.
- [31] H. Nguyen and R. Zheng, "Influence spread in large-scale social networks—a belief propagation approach," in *ECML-PKDD*, 2012.
- [32] T. E. Nichols and A. P. Holmes, "Nonparametric permutation tests for functional neuroimaging: a primer with examples," *Human brain mapping*, 2002.
- [33] R. Pamfil, N. Sriwattanaworachai, S. Desai, P. Pilgerstorfer, K. Georgatzis, P. Beaumont, and B. Aragam, "Dynotears: Structure learning from time-series data," in *AISTATS*, 2020.
- [34] W. D. Penny, "Comparing dynamic causal models using aic, bic and free energy," *Neuroimage*, 2012.
- [35] A. Pickering, "The cybernetic brain," in *The Cybernetic Brain*, 2010.
- [36] A. S. Potter, S. L. Dube, L. C. Barrios, S. Bookheimer, A. Espinoza, S. W. Feldstein Ewing, E. G. Freedman, E. A. Hoffman, M. Ivanova, H. Jefferys, E. C. McGlade, S. F. Tapert, and M. M. Johns, "Measurement of gender and sexuality in the adolescent brain cognitive development (abcd) study," *Developmental Cognitive Neuroscience*, 2022.
- [37] A. Riaz, M. Asad, S. M. M. R. Al-Arif, E. Alonso, D. Dima, P. Corr, and G. Slabaugh, "Fcnet: A convolutional neural network for calculating functional connectivity from functional mri," in *Connectomics in Neuroimaging*, 2017.
- [38] M. Rubinov and O. Sporns, "Complex network measures of brain connectivity: uses and interpretations," *Neuroimage*, 2010.
- [39] J. Runge, "Causal network reconstruction from time series: From theoretical assumptions to practical estimation," *Chaos*, 2018.
- [40] S. Saetia, N. Yoshimura, and Y. Koike, "Constructing brain connectivity model using causal network reconstruction approach," *Frontiers in Neuroinformatics*, 2021.
- [41] T. D. Satterthwaite, M. A. Elliott, K. Ruparel, J. Loughead, K. Prabhakaran, M. E. Calkins, R. Hopson, C. Jackson, J. Keefe, M. Riley, F. D. Mentch, P. Sleiman, R. Verma, C. Davatzikos, H. Hakonarson, R. C. Gur, and R. E. Gur, "Neuroimaging of the Philadelphia Neurodevelopmental Cohort," *NeuroImage*, 2014.
- [42] T. D. Satterthwaite, D. H. Wolf, D. R. Roalf, K. Ruparel, G. Erus, S. Vandekar, E. D. Gennatas, M. A. Elliott, A. Smith, H. Hakonarson, R. Verma, C. Davatzikos, R. E. Gur, and R. C. Gur, "Linked Sex Differences in Cognition and Functional Connectivity in Youth," *Cerebral Cortex*, 2015.
- [43] S. H. Siddiqi, K. P. Kording, J. Parvizi, and M. D. Fox, "Causal mapping of human brain function," *Nature reviews neuroscience*, 2022.
- [44] S. M. Smith, "The future of fmri connectivity," *Neuroimage*, 2012.
- [45] S. M. Smith, K. L. Miller, G. Salimi-Khorshidi, M. Webster, C. F. Beckmann, T. E. Nichols, J. D. Ramsey, and M. W. Woolrich, "Network modelling methods for FMRI," *NeuroImage*, 2011.
- [46] P. Spirtes, C. N. Glymour, R. Scheines, and D. Heckerman, *Causation, prediction, and search*, 2000.
- [47] K. E. Stephan and K. J. Friston, "Analyzing effective connectivity with functional magnetic resonance imaging," *Wiley Interdisciplinary Reviews: Cognitive Science*, 2010.
- [48] N. R. Swanson and C. W. Granger, "Impulse response functions based on a causal approach to residual orthogonalization in vector autoregressions," *JASA*, 1997.
- [49] G. J. Woeginger, *Exact Algorithms for NP-Hard Problems: A Survey*, 2003.
- [50] M. Xia, J. Wang, and Y. He, "Brainnet viewer: a network visualization tool for human brain connectomics," *PLoS one*, 2013.
- [51] R. Xu, Y. Yu, C. Zhang, M. K. Ali, J. Ho, and C. Yang, "Counterfactual and factual reasoning over hypergraphs for interpretable clinical predictions on ehr," in *Machine Learning for Health 2022*, 2022.
- [52] C. Yang, P. Zhuang, W. Shi, A. Luu, and P. Li, "Conditional structure generation through graph variational generative adversarial nets," *NeurIPS*, vol. 32, 2019.
- [53] Y. Yang, Y. Zhu, H. Cui, X. Kan, L. He, Y. Guo, and C. Yang, "Data-efficient brain connectome analysis via multi-task meta-learning," *KDD*, 2022.
- [54] Y. Yu, J. Chen, T. Gao, and M. Yu, "Dag-gnn: Dag structure learning with graph neural networks," in *ICML*, 2019.
- [55] Y. Yu, S. Zuo, H. Jiang, W. Ren, T. Zhao, and C. Zhang, "Fine-tuning pre-trained language model with weak supervision: A contrastive-regularized self-training approach," *arXiv preprint arXiv:2010.07835*, 2020.
- [56] Y. Zhang and H. Huang, "New graph-blind convolutional network for brain connectome data analysis," in *IPMI*, 2019, pp. 669–681.
- [57] X. Zheng, B. Aragam, P. K. Ravikumar, and E. P. Xing, "Dags with no tears: Continuous optimization for structure learning," *NeurIPS*, 2018.
- [58] Y. Zhu, H. Cui, L. He, L. Sun, and C. Yang, "Joint embedding of structural and functional brain networks with graph neural networks for mental illness diagnosis," *EMBC*, 2021.